Dynamics of tall building of cross-laminated timber under service loadings: findings from the finite element model updating

Blaž Kurent, Boštjan Brank*

University of Ljubljana, Faculty of Civil and Geodetic Engineering, Jamova c. 2, SI-1000 Ljubljana, Slovenia

Wai Kei Ao, Aleksandar Pavic

University of Exeter, College of Engineering, Mathematics and Physical Sciences, Kay Building, North Park Road, Exeter, EX4 4QF, UK

Abstract

Dynamic identification of seven-storey cross-laminated timber (CLT) building in Glasgow,UK was performed based on forced vibration test. In this work, the corresponding findings of finite element model updating will be reported. A detailed finite element (FE) model with CLT walls and floors modelled by a fine mesh of layered shell elements. The connections were not explicitly included, while calibration of parameters FIX: is it equivalent stiffness calibration? avoid to use "some" in academic writing were chosen to accommodate for FIX: minimising? the resulting modelling error in the process of the updating. This adopted approach FIX: what is "this" adopted approach? is it related to equivalent stiffness calculation? provided an excellent correlation between numerical simulation and experimental measurement in the first six modes eigen-properties(natural frequencies and mode shapes). Moreover, the results of sensitivity analysis and model updating showed a reduction of the vertical (axial and bending) stiffness of the walls due to the wall-floor joint effect. In addition, the in-plane shear flexibility of the CLT floors showed up significant influence on the higher order eigenmodes. Another finding of this study is the modelling of the building foundation based on the FRF-based measurement result of low frequency ranges and small amplitude excitations was not requested in this building. These findings could provide suggestions on how to prepare a FE model for better serviceability analysis of medium-high-rise CLT buildings under dynamic service loadings FIX: loading or loading's'? because you only mentioned wind , e.g. wind.

Keywords: Tall timber building, Cross-Laminated Timber (CLT), dynamic service loadings, forced vibration tests, modal parameters, spatial aliasing, finite element model updating

1. Introduction

Tall Timber Buildings (TTBs) have structural elements made from either Cross-Laminated Timber (CLT) or Glued-Laminated Timber. Some TTBs have their load-bearing structure made entirely of

*corresponding author; bbrank@fgg.uni-lj.si

wood and connections, which is in contrast with hybrid TTBs that constructed reinforced concrete and/or steel with timber structural elements. An example is seven-storey residential building in Glasgow, called Yoker, see Figure 1, which was the tallest Scottish timber building ~~that~~ constructed in 2017. In this TTBs made entirely of CLT, the connected CLT panels form the walls and floors.

With the increasing number of TTBs, more experimental data on the dynamics of various types of TTBs under service loadings, wind in particular, is getting available from ambient vibration test [26, 34] FIX: I just left AVT here since these two references were discussed ambient only, not force vibration test. Also, Saule paper is still not published yet, do you think it should be here for reference . The experimental research provides correlated modal properties for tested TTB, i.e. natural frequencies, mode shapes and damping ratios. To get optimal results for the dynamic modal identification of TTBs under service loadings, combining experimental test and numerical simulation are mandatory. However, currently, the accuracy of FE models for modern TTBs subjected service loadings is poorly understood, mainly because of the lack of information and knowledge about the stiffness and damping.

For TTBs, the wind can generate vibrations that cause discomfort or annoyance to occupants due to the perceived horizontal swaying. Wind-induced vibrations can also generate undesirable peak acceleration levels. For these reasons, the wind-induced dynamic excitation is becoming the governing design criteria ~~(besides the earthquake excitation in seismic regions)~~ for determining the size and shape of modern TTBs [11, 27]. Despite the practical importance of the problem, the dynamics of tall CLT buildings under service loadings has not attracted much research attention. From our best knowledge, there have been only a few journal publications on the topic, see [19, 4, 25, 27]. This is in contrast with the number of studies related to the performance of CLT buildings under seismic loadings, see [16, 19] for representative reports, limited dynamic loading analysis of CLT panels and connections, e.g. [22, 14, 35, 17], and aspects of design procedures, e.g. [7, 31, 20, 23].

The service loading related studies typically exploit the results of the ambient vibration tests, and perform FE/analytical analysis (or model updating), to identify dynamic properties of pure or hybrid CLT building. In [19], the first four eigenmodes were identified experimentally, and correlated with FE results, for a four-storey combination of CLT floors, glulam frames and light-frame walls. The authors concluded that non-structural building components played a significant role in the measured ambient vibration excitations. In [4], the first three eigenmodes were identified experimentally for eight-storey hybrid CLT building with reinforced concrete core, and a simple analytical model was proposed for model updating. In addition, the [4] paper suggested that the connections do not significantly contribute to the low-amplitude dynamics, and that the CLT floors behave like rigid diaphragms. However, this suggestion will be confirmed in the present study for Yoker building. In [25], the first three eigenmodes for five-storey CLT building with reinforced concrete core were identified and compared to FE results. In [27], the first natural frequency was estimated for seven-storey CLT building by taking into account overall building stiffness reduction due to the wall-floor joints, and compared with the measurements. The approach of this study for discussing dynamics of tall CLT building under service loadings differs from the above mentioned in two aspects: (i) It is based on forced vibration tests, and (ii) Detailed FE model of the building is used. In this work, the findings obtained from the FE model updating will be reported.

For CLT panels, the computer-controlled cutting techniques are usually used to precut openings for windows, doors and services. The panels are merged into a structural system with various types of steel connections and use screws or nails. Under large-amplitude dynamic loadings, such as seismic actions, the panels behaved as relatively rigid elements, and most of the deformation and energy dissipation took place in joints among the panels, e.g. [37, 14]. This is in contrast with low-amplitude dynamic service loadings, where the panels deformed mainly in shear and bending, e.g. [27, 14, 4]. In the joint FIX: which joint? floor to beam, beam to beam, beam to column? , there was typically a considerable friction, which required a certain level of force to overcome and mobilise the connections. During the seismic action, the connections will fully mobilise in the most of joints. However, there are also some joints, where friction may be small as an example of CLT floors, while an example of the joints with large friction may be the wall-floor joints. The joints with small friction may enable small sliding between panels, due to initial small gaps in connections during the service dynamic loadings with small amplitudes, such as wind.

The FE model updating that is based on vibration tests chosen parameters of the model are optimised so that the computed response better matches the experimentally measured dynamics. The use of the FE model for the FE model updating of Yoker building does not model connections, explicitly. In addition, the full connectivity between the panels is applied and taken into account the effects due to FIX: which joints? joints in a smeared manner. The first novelty of this work is to demonstrate the detailed FE modelling technique of a tall CLT building, which does not explicitly model connections among the CLT panels, but rather smears the effects due to joints, leads to an excellent matching between the experimental and numerical results. In particular, for Yoker building, the first six eigenmodes are matched almost exactly after the FE model updating.

By using the FE model updating that takes into account the effects due to joints in a smeared manner, two effects with significant impact on the overall stiffness of tall CLT structure could be identified. (i) The first effect is the wall-floor joint (see Figure 2b), where vertical timber fibres in the wall panel meet the horizontal timber fibres in the floor panel. These joints could reduce the overall stiffness of the walls. (ii) The second effect is related to the in-plane stiffness of the floors. Matching experimental and numerical higher frequencies showed considerable in-plane shear-flexibility of floors. This is the second important finding of this work that implies that assuming CLT floors behaved as rigid diaphragms may be inappropriate, depending on the shape of the building.

The experiments reported on the in-plane stiffness of single CLT panel and compositions of panels, e.g. [6, 10, 21, 30, 37], could provide insights into the in-iplane flexibility of CLT floors and walls. In [6], they studied in-plane shear stiffness of single CLT panels and described their behaviour as gross-shear or net-shear. They concluded that narrow-face bonded CLT panels with no cracks developed the gross-shear deformation mechanism and consequently had approximately 50 % higher shear moduli than CLT panels with cracks and/or gaps because the narrow faces were not glued, which developed net-shear. Moreover, the connections were the main contributing factor to the in-plane deformations of compositions of CLT panels, which was concluded in [10], based on sensitivity analysis of experimental results. In [37], two two-storey CLT structures were tested against lateral load, where the walls of the first and second structures were composed of large and small panels, respectively. For the latter case,

the initial stiffness was approximately 2/3 of the former structure (see Figure 14 in [37]). A difference of in-plane shear stiffness of three walls made of one, two and four panels was also reported in [21]. The aforementioned reports indicated that the in-plane shear stiffness of walls and floors in CLT building depended non-trivially on several factors, such as panel fabrication and boundary conditions (for a panel or composition of panels) that may influence on development of gross-shear or net-shear mechanism, number and orientation of panels in composition and connections. These uncertainties were also expressed in our findings from the FE model updating of Yoker building, with larger than expected in-plane shear stiffness of Yoker walls and much lower than expected in-plane shear stiffness of Yoker floors.

To check the influence of the foundation systems on the structural dynamics of Yoker building, the foundations were discussed and included into the FE model. The effects of the pile and pile-soil interaction were taken into account by three orthogonal FIX: linear? springs. Moreover, the interaction between the soil and foundation system FIX: I didn't get it, do you mean the pile cap? foundation system can be anything, should precisely tell readers above the piles was considered by the horizontal area springs FIX: what is area springs? spring is 2D point-point element, how to convert 2D area element, please explain clearly . The results of the FE model updating suggested that for low frequency ranges and small amplitude dynamic response, foundation modelling of Yoker building was not necessary required. FIX: did anyone/paper conduct similar study to discuss foundation modelling in structural design? Since this paragraph is lack of pass paper review

An important step in the model calibration is to quantify the extent of differences between the predicted and measured mode shapes. Most commonly used is the Modal Assurance Criterion (MAC) [3]. FIX: For problems with well-separated modes where sufficient degrees of freedom (DOFs) were measured <–I didn't understand this sentence , MAC value is a suitable measure for comparing experimental and numerical eigenvectors. However, when sensors did not capture enough motion of the system, modes could not be distinguished by MAC value alone. This phenomenon is called spatial aliasing FIX: are you sure the spatial aliasing meaning like this? please check the signal processing definition and read Ewin book section 3.6.3, the key word "sampling rate" and in Yoker testing the sampling rate is associated with the Nyquist frequency requirement and results in off-diagonal correlation in MAC matrix. A simple technique to avoid spatial aliasing FIX: The improvement of spatial aliasing could modify Nyquist frequency rather than place more sensors, and I guess you are trying to say the sensor position arrangement, right? they are different is placing sensors such that the off-diagonal terms of auto-MAC matrix are close to zero [12] FIX: please read carefully Ewin book p.256-258 you might find the answer on p.258 . More advanced methods of optimal sensor placement have been also developed in order to find locations that minimize off-diagonal terms of mass-weighted MAC matrix with certain number of sensors [18]. However, if spatial aliasing cannot be avoided, one needs to inspect auto-MAC matrix to ascribe non-negligible off-diagonal MAC terms to spatial aliasing [13]. Besides the information obtained from auto-MAC matrix, other measures of eigenvector correlation could be used to find matching modes. A simple graphical extension of MAC value was Frequency scaled Modal Assurance Criterion (FMAC) [13] that also took frequency into account for what?. Modal observability criterion (MOC) is another measure proposed for tackling spatial aliasing [36].

For Yoker building, we also had to deal with spatial aliasing, because the sensors were allowed to be placed only within the common areas of the building. It turned out that an extensive inspection of Auto-MAC matrix was enough to help us map numerical modes on experimental modes.

When considering parameters for the FE model updating, it is reasonable to select only those parameters that contribute the model's uncertainty to a number of degree. Sensitivity Analysis (SA) gives insight into a great preliminary exploration on FE model response due to a sequence of value variation of input parameters. The SA are usually divided into local and global methods. Local method gives an information about how the model responds when parameters are slightly changed in small vicinity of the reference point, whereas global method studies wider parameter space FIX: of what? . The local SA method could classify to one-at-a-time, Tornado diagram, and derivative-based methods. The global SA method could commonly have variance-based, regression-based, and density-based methods [5]. When deciding which methods to use, the goal of the SA should be precisely defined, which is often called the setting [29] FIX: what is the setting, even you explained, it is still not clear, please clarify!!! . In this study, factor prioritisation setting was adopted, where is variance-based SA (Sobol' method) that is a common choice FIX: common choice of the SA method? and the reason is? [29]. FIX: We use it for computation of first-order and total-effect sensitivity indices <– I don't understand this sentence.

The paper is organised as follows: After the introduction in Section 1, a seven-storey pure CLT timber building is briefly presented in Section 2. Section 3 describes an FE model of the building, which developed according to the best-engineering-judgement before the forced vibration test, and was mandatory for preparing pre-test planning. The experimental results are summarised in Section 4. Section 5 discusses the FE model updating procedure and analysis results, which is shown the selection of the updating parameters of the model. FIX: , with some of them chosen to take into account the effects of joints, allows for an efficient FE model updating without explicitly modelling connections <–I don't think this sentence here is making any sense, may deleted it or paraphrase it since I only guess the meaning here. In Section 6, the calibration of the FE model including foundation is discussed. Finally, the conclusions are drawn in Section 7.

2. Building description

The structural system of the seven-storey building (see Figure 1) that has T-shaped and is located in Glasgow, UK, and called Yoker, is completely made of CLT, apart from the reinforced concrete foundation system and ground floor slab, and a few steel beams and frames that were used to reinforce timber at different storeys. The characteristic dimensions of the building are: 31 m by 28 m in plan, 22 m in height above the ground floor slab, 3745 m^2 of the gross floor area, and 550 m^2 of the foot print area. Typical floor plan is shown in Figure 2a. The facade is simple and does not include any secondary load-bearing elements that could contribute to the structural stiffness of the walls. The soil layer under the building is made ground and alluvium strata (very soft to firm laminated clay) on part of the area. Beneath that is a layer of glacial till (stiff consistency grey sandy gravelly clay with cobbles/boulders), considered as appropriate foundation bearing material for the multi-storey

building. The foundation system will be described below in Section 6.

Five different types of CLT panels were used in construction, with thickness varying between 100 mm and 140 mm (except for the stair half landing, where 200 mm CLT panels where used), having either 3 or 5 layers, see Table 1. As shown in Figure 1b, the external walls (as well as some internal walls) are made out of large CLT panels, with pre-cut openings for windows, which have the height of the storey and the length of the edge of the building (except for the last storey, where this is not the case). The CLT panels in Yoker building are typically connected with combination of angle brackets and wood screws, see Figure 2 showing two examples of connections. The producer of CLT panels is Stora Enso, which provides mean material properties for their CLT panels (of C24 grade spruce) [2] as shown in Table 2. For comparison, Table 2 also includes the mean material properties provided by the code EN-338 for C24 spruce boards.

(a) Photo from November 2019.

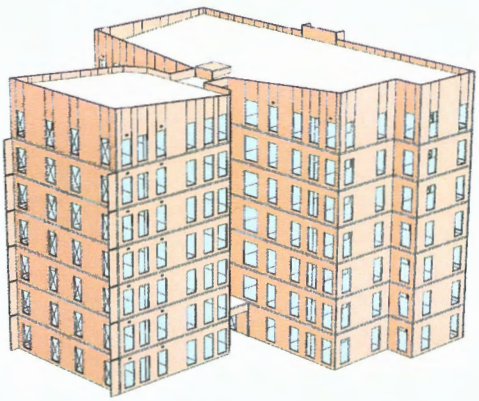

(b) Distribution of CLT panels for external walls.

Figure 1: Yoker, 7-storey CLT building in Glasgow, UK.

Table 1: Types of CLT panels used.

		Area [m^2]	
CLT panel type	Thickness [mm]	Walls	Floor/roof
SE-100-L3s/SE-100-C3s	100	1149	525
SE-100-L5s/SE-100-C5s	100	968	/
SE-120-L3s/SE-120-C3s	120	299	/
SE-120-L5s/SE-120-C5s	140	1909	2926
SE-140-L5s/SE-140-C5s	140	1109	190
SE-200-L5s	200	/	49

Table 2: Mean material properties for CLT (grade C24 spruce) and grade C24 spruce boards.

Property	Stora Enso	EN 338
Elastic modulus E_1 [MPa]	12 000	11 000
Elastic modulus $E_2 = E_3$ [MPa]	by EN 338	370
Shear modulus $G_{12} = G_{13}$ [MPa]	460	690
Shear modulus G_{23} [MPa]	50	/
Density ρ [kg/m^3]	470	420

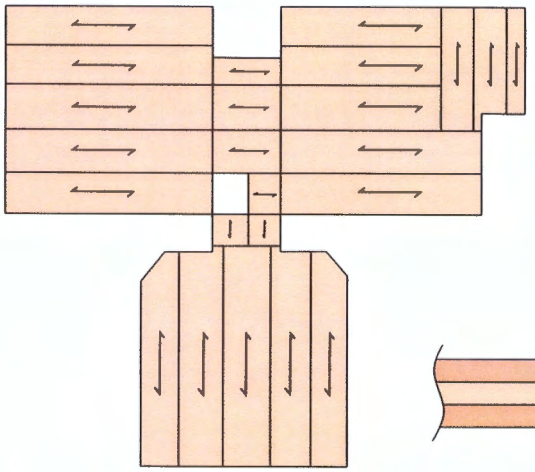

(a) Typical floor plan with CLT panels orientations and typical connection between the panels. This particular plan is for 4^{th} to 6^{th} storey.

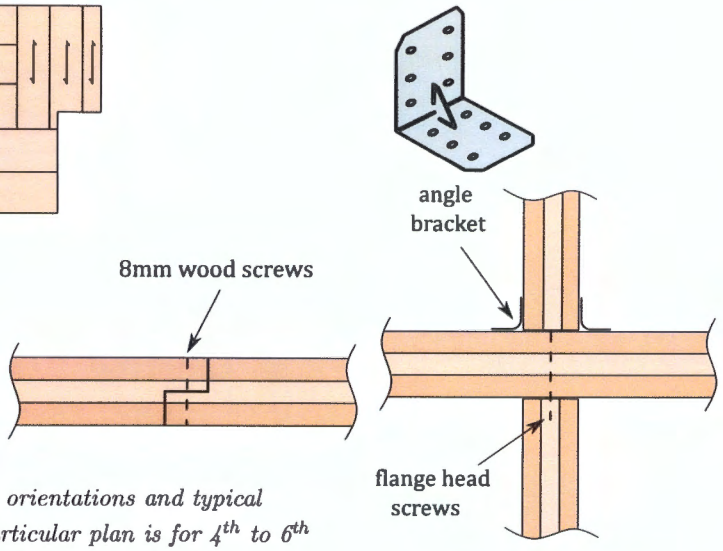

(b) Typical wall-slab joint.

Figure 2: Some details of Yoker building.

3. Initial finite element model

In this section we describe the initial (i.e. the best-engineering-judgement) FE model that is based on the following basic assumptions: (i) the foundation system is rigid and fixed, (ii) the connections can be neglected, (iv) the floors are flexible (i.e. the assumption of the rigid-diaphragm is not used).

3.1. Modelling CLT building by shell finite elements

For the construction of the FE model, Ansys software [1] is applied. Figure 3 shows a virtual geometric partition for the external walls and roof used in the FE modelling (the real partition with respect to the CLT elements is presented in Figure 1b), as well as detail of the FE mesh.

The CLT panels are modelled by multi-layer, four-node, shell element with six degrees of freedom per node (named SHELL181 in Ansys). Each layer has its associated thickness and orientation (with respect to the local coordinates x, y, z of the panel) that is used by the orthotropic material model, which is applied layer-wise. The orthotropic material model for the shells has six independent constants, e.g. [8, 9]. For the initial FE model, these constants are adopted as mean material values

provided by the CLT producer Stora Enso, see Table 2. Moreover, the sixth constant, Poisson's ratio ν_{12}, is assumed as 0.3 (different sources report the values between 0.1 and 0.72 ta številka ni realna, treba jo je popraviti, see [20], [28] and [33]). We note, however, that the value for ν_{12} has a small influence on the output of the model, see Section 5.4.

The mid-surfaces of the shell finite elements are placed in accordance with positions of the mid-planes of the CLT panels, as shown in Figure 4b. The joints between the panels are idealised as non-existing, meaning that the connections are not modelled. The FE mesh is restrained at the level of (the top surface of) the reinforced concrete ground floor, i.e. all degrees of freedom are restricted to zero at nodes at that level.

3.2. Modelling of the building stiffness

Structural elements that are included in the FE model as entities with stiffness are: the external and internal load-bearing walls, floors, roof, and elevator shaft. We neglect the steel beams and frames that locally reinforce timber at some storeys, which add up to less than 1 % of the total mass of the load-bearing structure, and have a negligible effect on the overall stiffness (as checked numerically). Moreover, we do not model the stiffness of the building elements that are traditionally treated as the non-load-bearing when considering building structural system (e.g. staircase and windows), as well as non-load-bearing partition walls. We note that those partition walls represent approximately 6 % of the total mass of the walls in a storey.

3.3. Modelling of the building mass

The mass of the well-documented non-structural building elements (i.e. facade, insulation, screed, flooring, fireline board, cladding, and non-load-bearing partition walls) is taken into account as uniformly distributed area mass over walls and floors. More specifically, the sum of masses of non-structural elements attached to the walls within a particular storey is smeared over the FEs that model the walls in that storey. Similarly, the sum of masses of non-structural elements attached to the floor is smeared over the FEs that model the particular floor. Furthermore, the mass of all undocumented building elements with uncertain weights (such as windows, doors, steel stairs), documented but unevenly distributed elements (various steel structural elements) and uncertain live load (such as furniture, residents, etc.). are combined into one parameter - uncertain mass - that is estimated to $q = 25\,\mathrm{kg/m^2}$. It is distributed over the FEs that are modelling the floors (it is not distributed over the ground floor and roof), in particular, over the apartment areas (it is not distributed over the corridors). An estimated initial mass of the building (excluding reinforced concrete foundation system and ground floor) is 1270 t and can be assigned to the following contributions: around 515 t to the timber part of the building, around 685 t to well-documented non-structural elements and around 70 t of uncertain mass.

3.4. Convergence analysis

The convergence analysis was performed in order to find an optimal mesh. To that end, the natural frequencies were computed by modal analysis for nine different FE meshes. The results are shown

in Figure 5, where the convergence is presented for the first six natural frequencies in terms of the relative difference $\Delta_i(\mathcal{M})$. The latter is defined for the i-th natural frequency f_i and mesh $\mathcal{M}$ as:

$$\Delta_i(\mathcal{M}) = \frac{f_i(\mathcal{M}) - f_i(\mathcal{M}_f)}{f_i(\mathcal{M}_f)} \tag{1}$$

where $\mathcal{M}_f$ denotes the finest chosen mesh with 2.79×10^6 nodes. Figure 5 shows that finer meshes lower natural frequencies. For the subsequent work, we choose the mesh M_a with 2.61×10^5 nodes, as a reasonable trade-off between the accuracy and computational time. By assuming that the finest chosen mesh M_f yields converged results, the approximate discretization error

$$\Delta_i(\mathcal{M}_a) = \frac{f_i(\mathcal{M}_a) - f_i(\mathcal{M}_f)}{f_i(\mathcal{M}_f)} \tag{2}$$

can be computed for the applied mesh M_a. The following numbers are obtained for the first six natural frequencies, respectively: 1.10 %, 0.82 %, 1.14 %, 1.29 %, 0.87 %, 0.69 %.

3.5. Natural frequencies and mode shapes

Table 3 presents the first six mode shapes and related natural frequencies, obtained by the modal analysis for the applied mesh. We adopt the ordering based on the match with experimental modes as shown in Section 4.2 and Table 4. The first three modes are very closely spaced in terms of frequencies, which hinders its matching to experimental modes. The 1st mode is a simple bending mode in the weaker building direction. The 2nd and the 3rd modes are torsion (almost a mirroring) modes. Mode 4 is more complex torsion mode that exhibits a relative motion between the two building parts (hereinafter denoted as the "web" and the "flange" of the T-shaped building). Mode 5 is shear mode with some bending that shows, along with modes 4 and 6, in-plane deformations of floor slabs. The 6th mode is another bending mode, though a higher-order one, with some torsion.

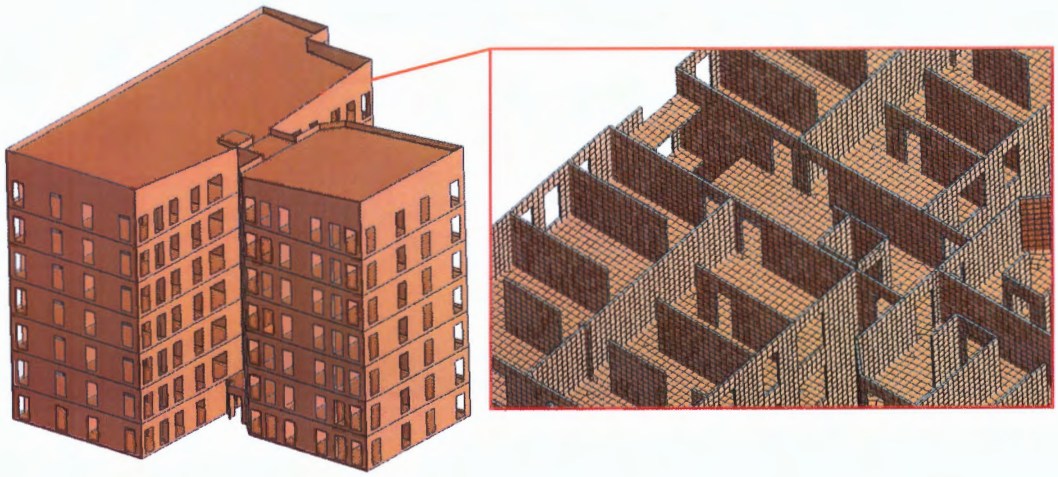

Figure 3: FE model geometry (left) and detail of the FE mesh (right).

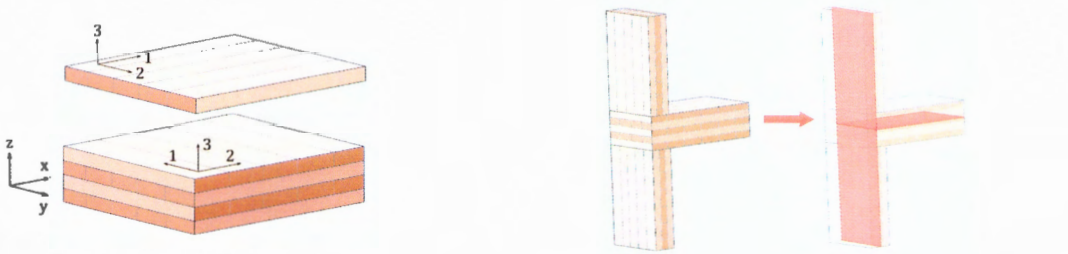

(a) Layers of CLT panel.

(b) CLT panels and mid-surfaces of shell elements.

Figure 4: CLT panel (left) and modelling detail (right).

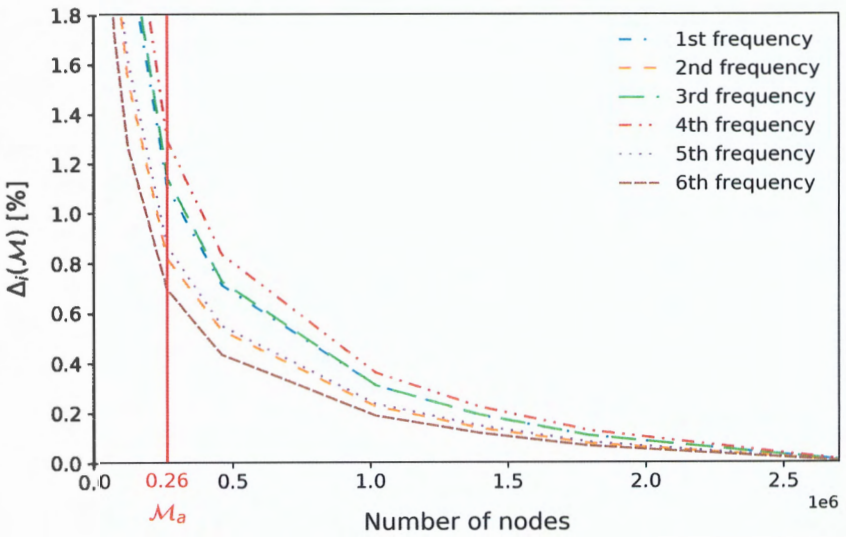

Figure 5: Convergence analysis results.

Table 3: First six FE mode shapes and respective deformations of the 6^{th} floor. Note that the experimental mode order is adopted.

Mode	Frequency	Mode shape	6^{th} floor deformation
1	2.85 Hz	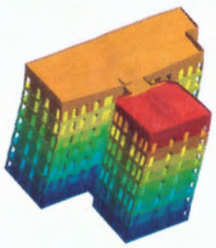	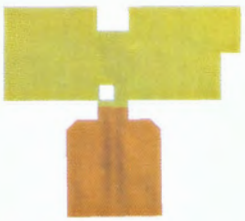
2	2.81 Hz	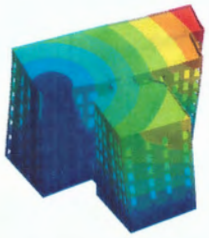	
3	2.94 Hz	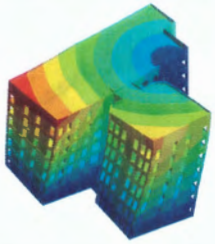	
4	3.98 Hz	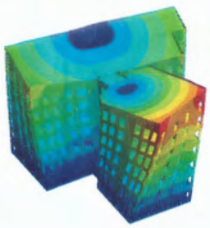	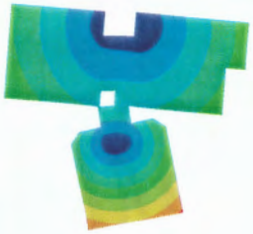
5	8.32 Hz	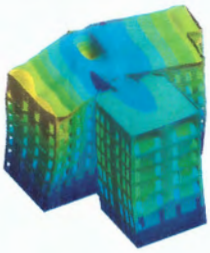	
6	8.19 Hz	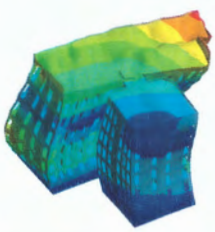	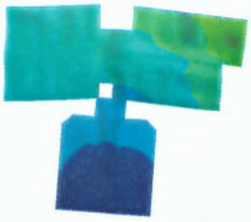

4. Experimental results

A brief information of in-situ forced vibration test of Yoker Building is summarized in this section. Some experimental results are compared with numerical, and further detail of experimental results will be presented in authors another publication.

4.1. Vibration testing

Based on the information, gained from the initial FE model, appropriate vibration testing setup and layout were selected. For the excitation, three synchronised APS Model 400 electrodynamic shakers with total moving mass of 68.85 kg were placed on the 6th floor. For measuring accelerations Honeywell QA750 and Japan Aviation Electronics Industry, Limited JA-70SA accelerometers were used. Altogether 13 sensor locations were chosen with 2 sensor locations at each floor (no sensors were placed on the ground floor) and one additional in the 6th floor as a reference sensor near the shakers. Each sensor location measured acceleration in two horizontal directions, as shown in Figure 6.

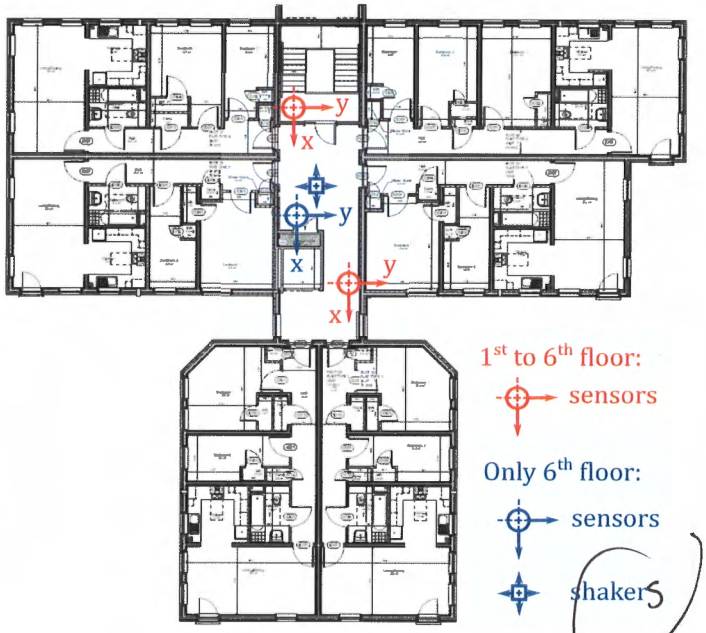

Figure 6: Layout of shakers and sensors

The building was operational at the time of the measurements, so the placement of the sensors was limited to the corridors in the core of the building. Since the measured degrees of freedom do not give sufficient information of the motion of the whole building (see e.g. the 4th to 6th mode in Table 3), some degree of spatial aliasing is expected.

Two sets of random excitation vibration tests were carried out, one with shakers exciting in x direction and the other in y direction (see Figure 6 for the directions). The average amplitude of the total force was in 500 N and near shaker location had average structural response 0.005 m/s^2 and 0.004 m/s^2 in the x and y directions, respectively. Excitation signal was wide frequency bandwidth white noise

(0-10 Hz). Single-input multiple-output modal identification method (Complex Mode Indicator Function (CMIF)) was used to identify 8 modes. Measured natural frequencies are presented in Table 4 and compared with the FE results.

Table 4: Comparison of initial FE model and experimental results.

Experiment		Initial FE model		
i	Frequency	j	Frequency	MAC_i
1	2.85 Hz	2	2.85 Hz	0.77
2	2.93 Hz	1	2.81 Hz	0.77
3	3.13 Hz	3	2.94 Hz	0.38
4	3.63 Hz	4	3.98 Hz	0.95
5	6.73 Hz	6	8.32 Hz	0.80
6	8.74 Hz	5	8.19 Hz	0.78
7	9.68 Hz		/	
8	11.9 Hz		/	

4.2. Comparison of experimental and numerical results

~~In order to compare the natural frequencies, one should first match corresponding experimental and numerical mode shapes.~~ Commonly used measure for correlation between two sets of modes is modal assurance criterion (MAC) calculated as:

$$\mathrm{MAC}(\psi_{i,e}, \psi_{j,n}) = \frac{\left|\psi_{i,e}^T \psi_{j,n}^*\right|^2}{\left(\psi_{i,e}^T \psi_{i,e}^*\right)\left(\psi_{j,n}^T \psi_{j,n}^*\right)}, \tag{3}$$

where $\psi_{i,e}$ and $\psi_{j,n}$ are i-th experimental and j-th numerical mode shape, respectively, and $*$ denotes conjugation of complex mode shapes. MAC value 1 suggests strong ~~correlation~~ between two modes, whereas value 0 suggests no ~~correlation~~. Commonly, all experimental and numerical mode shapes are compared pair-by-pair and presented in MAC matrix, which is ideally diagonal, unity matrix.

In our case, MAC matrix is far from diagonal and ~~suggests~~ too many correlated mode shapes, see Figure 7. ~~This can be attributed to the following causes arising from measurements [3]: (i) noise of the measuring setup, (ii) measured mode shapes are result of forced excitation other then the desired input (e.g. wind during the measurement might disrupt the results), (iii) insufficient data stemming from too few measured degrees of freedom. The latter usually falls under the term spatial aliasing,~~ which can happen not only when too ~~little~~ sensors are used but also when they are placed so that not enough ~~motion is captured~~. ~~In our case, poor sensor placement can be suspected already from the layout presented in Figure~~ 6. Spatial aliasing ~~is~~ confirmed by examining Auto-MAC matrices in Figure 8, which display many non-zero off-diagonal terms.

With spatial aliasing, additional information is needed to find matching pairs of modes. Sometimes, a criterion that combines MAC value and frequency is used [24], but in our case, frequencies in question are so close ~~together~~ that such criterion does not separate between a good and a bad mode pair.

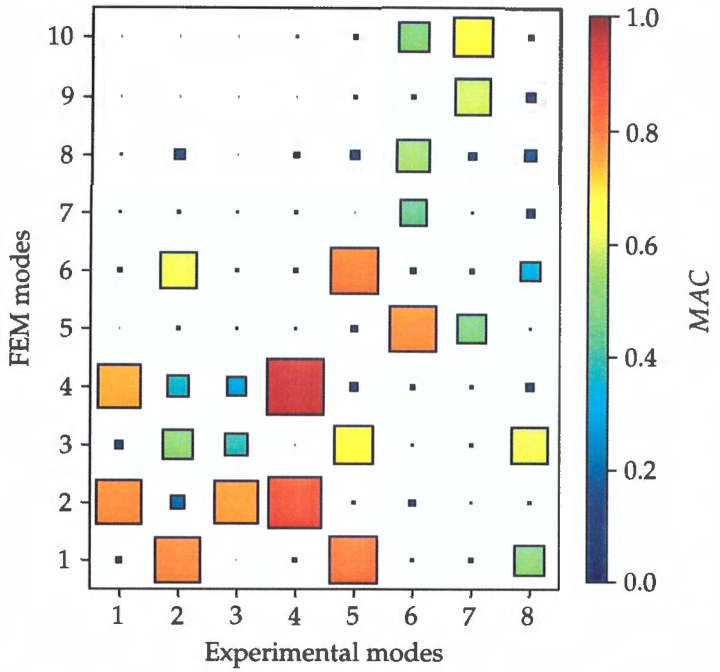

Figure 7: MAC matrix for the initial FE model.

We use Auto-MAC matrices in order to find matching mode pairs. First, ~~we compare~~ MAC matrix with experimental Auto-MAC matrix, ~~shown in~~ Figure ~~7 and~~ 8a, ~~respectively~~. ~~We try to find the pairs of experimental and FE modes that show similar correlation with experimental modes. In effect, we search for resembling rows while also having in mind what frequencies are linked to the modes. For example~~, the 1st row of experimental Auto-MAC matrix strongly resembles the 2nd row of MAC matrix, but it is very similar to the 4th row of MAC matrix. Comparing also the frequencies of those modes, we can confidently say that the 1st experimental mode matches the 2nd FE mode. In a similar fashion, we connect 2nd experimental to 1st FE mode, 4th experimental to 4th FE mode, 5th experimental to 6th FE mode, and 6th experimental to 5th FE mode. Leaving us with the only reasonable connection left between 3rd experimental and 3rd FE mode. The pairs can also be confirmed by comparing the columns of FE Auto-MAC matrix in Figure 8b with the columns of MAC matrix.

We note that even though some MAC values in Table 4 are not sufficiently high and frequency differences are too large for definite pairing of modes, we match them for the purpose of model updating and later comparison. We also note that the experimental modes 7 and 8 could not have been matched with sufficient level of trust even after update of the initial FE model.

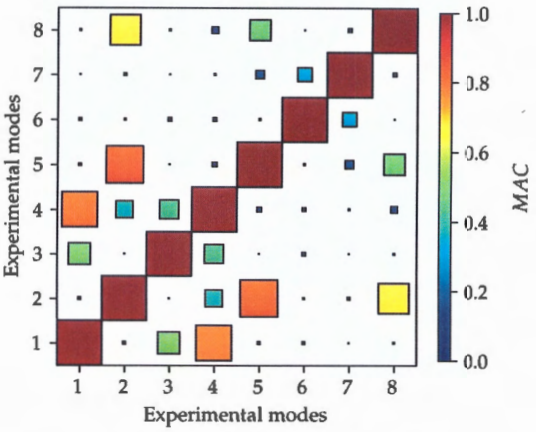

(a) For experimental mode shapes.

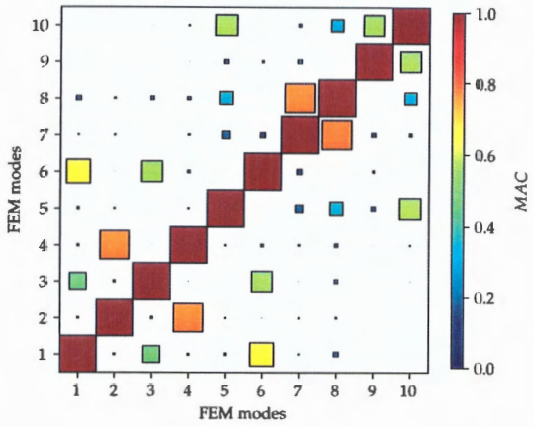

(b) For numerical mode shapes.

Figure 8: Auto-MAC matrices.

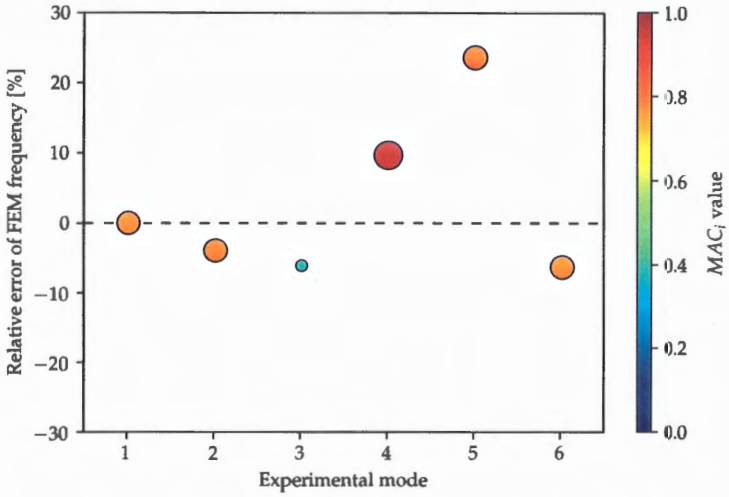

Figure 9: FMAC plot for the initial FE model.

5. Model updating

In this section, we describe the process of FE model updating for Yoker, and we discuss the results.

5.1. Parameters selection

After the initial screening sensitivity analysis for linear effects of several parameters, we could conclude that the following parameters of the initial FE model are important: elastic modulus in the direction of fibres E_1, in-plane shear modulus G_{12}, timber density ρ, and uncertain mass q. These parameters influence the natural frequencies and mode shapes considerably. We could also conclude that the following parameters of the initial FE model has small influence on the results: elastic modulus in the

weaker direction E_2, both out-of-plane shear moduli (G_{13} and G_{23}), and Poisson's ratio ν_{12}. Moreover, we also eliminated the timber density as a suitable candidate, since it has a similar effect on the results as uncertain mass q.

Table 5: Parameters used in sensitivity analysis and model updating.

Parameter	Range	Property	Application
e_1	6–12 GPa	E_1	Used for CLT panels in walls. Only for layers with fibres in vertical direction.
e_2	10–13 GPa	E_1	Used for CLT panels in walls. Only for layers with fibres in horizontal direction.
e_3	6–12 GPa	E_1	Used for CLT panels in floor slabs. All layers.
g_1	400–750 MPa	G_{12}	Used for CLT panels in walls. All layers.
g_2	200–500 MPa	G_{12}	Used for CLT panels in floor slabs. All layers.
q	5–100 $\mathrm{kg\,m^{-2}}$	Mass	Additional distributed mass along all floors.

Six parameters are chosen for more elaborated sensitivity analysis and FE model updating, see Table 5. We note that we introduced different parameters for the same material moduli. In particular, g_1 represents G_{12} for the layers of CLT panels in walls, and g_2 represents G_{12} for the layers of CLT panels in floors. Moreover, e_1 and e_2 represent E_1 for the layers of CLT panels in walls in vertical and horizontal direction, respectively, and e_3 denotes E_1 for the layers of CLT panels in floors. The reason is the aim to accommodate two panel-connection effects in a smeared sense, without explicitly modelling connections. Thus, we know in advance that after the updating some of the parameters from Table 5 will not represent the material property, because they will be polluted with the modelling error.

The chosen ranges of the parameters from Table 5 reflect not only the material data information provided by the producer of CLT panels Stora Enso (and EN-338), see Table 2, but also allow capturing the stiffness reduction of walls and floors because of the effects described below. The range for uncertain mass parameter is estimated to take into account uncertainty in non-structural building elements, whose weight is not well documented, uncertain live loads (present during the measurements), and also uncertainty of timber density.

5.2. Modelling of effect of wall-floor joint

Let us inspect the floor contribution to the stiffness of the wall because of the wall-floor joint (see Figure 2b). The effect on the vertical axial stiffness is illustrated in Figure 10, where we consider a unit width of one-storey of the wall as a compressed bar supported at the bottom end and imposed to unit displacement at the top end. The bar consists of vertical CLT (denoted as A) and horizontal CLT (denoted as B). It is discretized with: (i) two bar FEs with elastic moduli E_0 and E_{90} for element

A and B, respectively, and (ii) one bar FE with effective elastic moduli μE_0. By equating the force needed to produce the unit displacement, one can get the value for μ. Figure 11 shows μ as a function of γ, which takes into account the effective width in floor CLT, and as a function of α, which takes into account different configurations of CLT panels from Table 1 used for the walls ($\alpha \in [0.6, 0.7]$). It can be seen that μ is in the range between approximately 0.5 and 0.7 for γ being between 1 and 2.

We expect that when the wall-floor joint is modelled as in Figure 4b, the axial vertical stiffness of the wall FEs reduces approximately for factor μ, which will capture the parameter e_1. Moreover, e_1 will capture also reduction of the bending stiffness of the wall FEs.

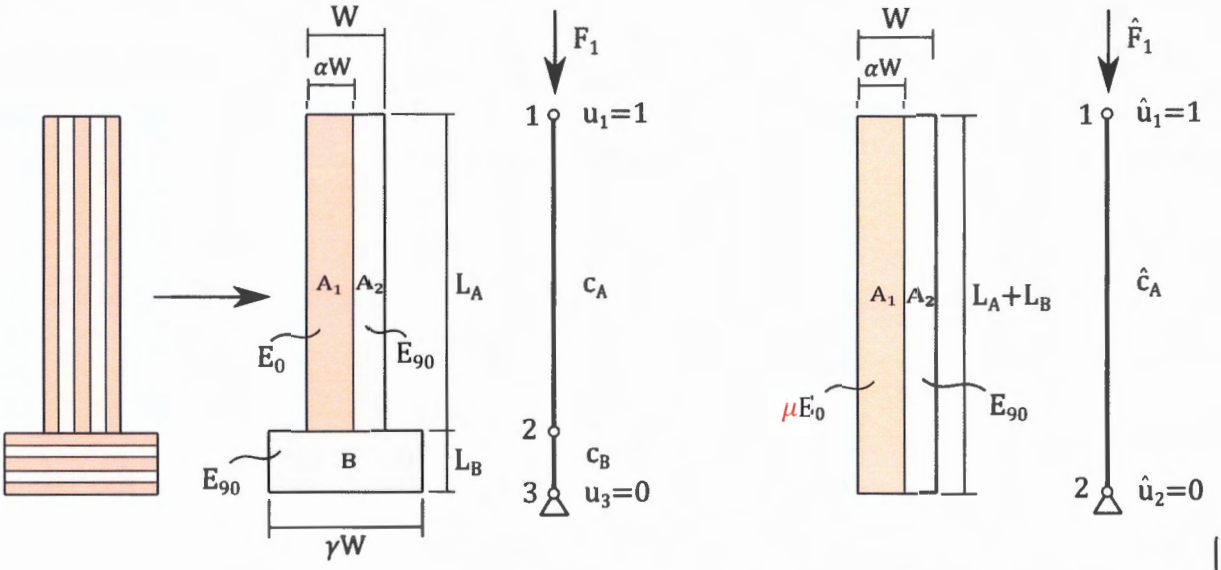

$$c_A = \frac{E_0 \alpha W}{L_A} + \frac{E_{90}(1-\alpha)W}{L_A}$$

$$c_B = \frac{E_{90}\,\gamma\,W}{L_B}$$

$$\begin{Bmatrix} F_1 \\ F_2 = 0 \\ F_3 \end{Bmatrix} = \begin{bmatrix} c_A & -c_A & 0 \\ -c_A & c_A + c_B & -c_B \\ 0 & -c_B & c_B \end{bmatrix} \begin{Bmatrix} u_1 = 1 \\ u_2 \\ u_3 = 0 \end{Bmatrix}$$

$$\hat{c} = \frac{\mu\, E_0\, \alpha\, W}{L_A + L_B} + \frac{E_{90}\,(1-\alpha)\,W}{L_A + L_B}$$

$$\begin{Bmatrix} \hat{F}_1 \\ \hat{F}_2 \end{Bmatrix} = \begin{bmatrix} \hat{c} & -\hat{c} \\ -\hat{c} & \hat{c} \end{bmatrix} \begin{Bmatrix} \hat{u}_1 = 1 \\ \hat{u}_2 = 0 \end{Bmatrix}$$

$$F_1 = \hat{F}_1 \implies \mu = \mu(\alpha, \gamma)$$

Equations must be numbered.

Figure 10: Illustration of the effective axial vertical stiffness of the wall due to the wall-floor joint (note that $E_0 = E_1$ and $E_{90} = E_2$).

5.3. Modelling of effect of floor connections

The in-plane flexibility of the floors affects the load distribution between the walls, and adds to local deformations and inter-storey drift, thus affecting the overall response of the building. For a composition of CLT panels, the in-plane flexibility depends on their number, size and disposition, e.g. [21, 37], with connections as the main contributing factor, e.g. [10]. The friction between the CLT panels in floors may not be large, and for vibrations with small amplitudes small slips between the

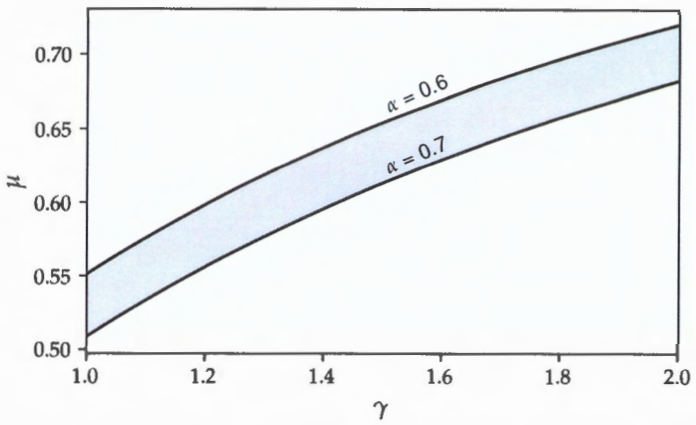

Figure 11: Domain of values for factor μ from Figure 10.

panels may be enabled (that do not mobilise much the connections) for some deformation modes.

The FE models for tall CLT buildings usually adopt assumption that floors behave as rigid diaphragms, e.g. [4, 19, 25], thus neglecting even deformability of the CLT panels, let alone the connections. In our FE model, the CLT panels are modelled as flexible, but the connections between the panels are neglected. In order to enable modelling the effect of connections between the floor CLT panels in a smeared sense, two parameters, g_2 and e_3, are introduced, which will reduce the in-plane shear and axial stiffness of floor FEs.

5.4. Sensitivity analysis

Sensitivity analysis was performed in order to analyse the influence of the parameters from Table 5 on natural frequencies and MAC values for the first six modes. We carried out variance-based sensitivity analysis by computing first-order and total effect sensitivity indices. This method is sometimes called Sobol' method or Sobol' variance decomposition, e.g. [29]. First-order sensitivity index tells us what fraction of total variance $V(Y)$ of response Y can be attributed to parameter X_i. It is computed through the expected value $E_{\sim X_i}(Y|X_i = x_i^*)$ of response Y over all parameters except X_i at fixed value $X_i = x_i^*$. Large variance of this expected value $V_{X_i}(E_{\sim X_i}(Y|X_i))$ over parameter space of X_i implies a high influence of parameter X_i on the response Y. First-order sensitivity index is computed as a ratio between conditional and total variance:

$$S_i = \frac{V_{X_i}(E_{\sim X_i}(Y|X_i))}{V(Y)}. \tag{4}$$

Another measure of importance of specific parameter is total effect term. This includes all higher order terms capturing also interactions between the parameters. Total effect sensitivity index S_{Ti} is defined in the following way:

$$S_{Ti} = 1 - \frac{V_{\sim X_i}(E_{X_i}(Y|X_{\sim X_i}))}{V(Y)}. \tag{5}$$

Now we compute the expected value of the response Y over parameter X_i by fixing all but X_i parameter and find its variance over all parameters except X_i. If the values of S_i and S_{Ti} are close to zero, parameter X_i does not have much influence on the response Y. Higher the values of S_i and S_{Ti} greater the influence of the parameter X_i on the response Y. If the values of S_i and S_{Ti} are similar, there is little interaction of parameter X_i with other parameters. Also, if the sum of all terms S_i is equal to 1, model is said to be additive and there is little interaction between the parameters.

Total number of runs of FE model in this method is defined as $N(k+2)$, where N is called base sample (usually chosen around 500-1000) and k is number of parameters. We have chosen N to be 500, which for $k = 6$ parameters results in 4000 total runs of the FE model that needed roughly two weeks to be evaluated (using 12 core PC). We used open source python library SAlib [15] to carry out the sensitivity analysis. Results are shown in Figure 12.

Comparing sensitivity plots from Figures 12a and 12c, we can conclude that the parameters influence first six natural frequencies fairly independently. Namely, the indices S_{Ti} are very close to S_i. The parameter g_1 has strong influence on all but 5^{th} natural frequency. In contrast, g_2 strongly influences 5^{th}, moderately 4^{th}, slightly 6^{th}, and has negligible effect on the first three frequencies. The parameter e_1 has a moderate effect on the first natural frequency and some impact on the other frequencies, except on the 5^{th}, where its effect is negligible. The parameter e_2 has a negligible effect on natural frequencies. The same can be said for the parameter e_3 for the first three frequencies, while e_3 has a small impact on the last three frequencies. Lastly, q has a low to moderate effect on all natural frequencies.

In contrast, high interaction between the parameters in the effect on MAC_i values is present, where MAC_i denotes i-th matching mode pair of the experimental and numerical natural frequency. Figures 12b and 12d show that the total-effect indices S_{Ti} are much higher than the first-order indices S_i. This means that the effect of one parameter on the response will depend on the values of other parameters. More specifically, g_1 and e_1 have strong influence on MAC_1, MAC_2 and MAC_3 with high mutual interaction. MAC_4 is influenced mostly by g_1 and slightly by e_3, but no interaction is present. Lastly, MAC_5 and MAC_6 are influenced by all the parameters except e_2 with high level of mutual interaction between the parameters.

5.5. Model updating

The FE model updating is an optimization procedure, which computes the values of the optimization parameters such that the difference between the predicted response (e.g. the FE model results) and experimentally measured response is minimized. In our study, we take into account natural frequencies and MAC values for the first six vibration modes. Two measures of difference between the predicted and measured response are applied. One relates to the similarity of the mode shapes:

$$\delta_{MAC} = \sum_{i=1}^{6} (1 - MAC_i)^2, \tag{6}$$

and the other relates to the difference in natural frequencies:

$$\delta_{freq} = \sum_{i=1}^{6} \left(\frac{f_{i,exp} - f_{i,FEM}}{f_{i,exp}} \right)^2. \tag{7}$$

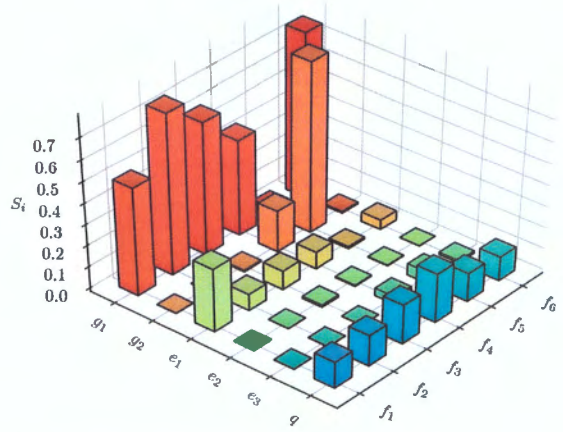

(a) First order sensitivity indices for natural frequencies.

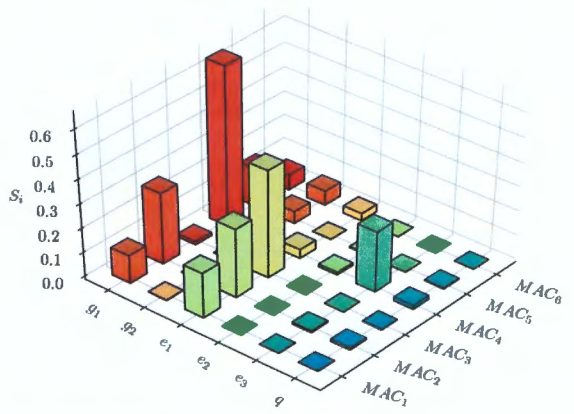

(b) First order sensitivity indices for MAC values.

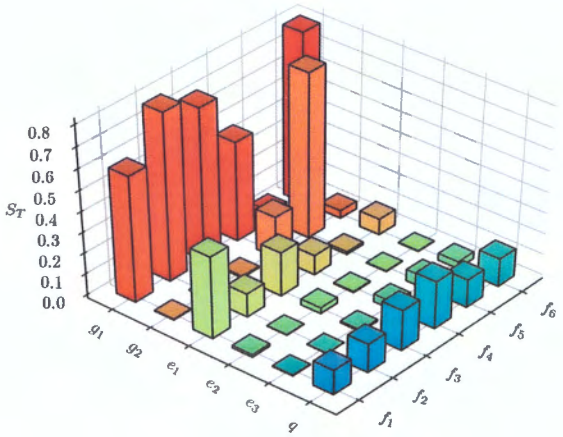

(c) Total effect sensitivity indices for natural frequencies.

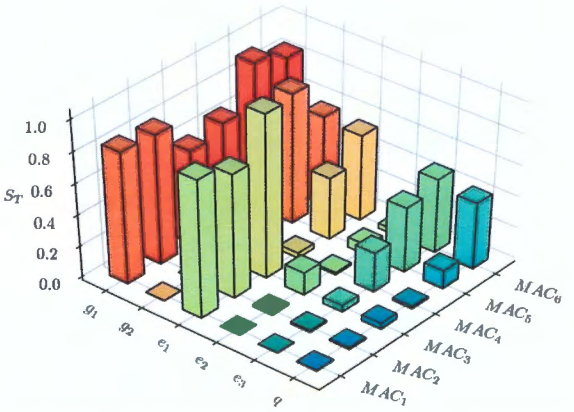

(d) Total effect sensitivity indices for MAC values.

Figure 12: First order and total sensitivity indices.

where $f_{i,exp}$ and $f_{i,FEM}$ are the experimental and numerical natural frequency of i-th matching mode pair, respectively. Recall that the chosen optimization parameters and their bounds are shown in Table 5, and there are no other constraints.

The optimization was performed by using optimization tools incorporated in Ansys. In particular, we applied multi-objective genetic algorithm with 200 initial samples, 15 maximum iterations, and with 100 samples per each iteration. Maximum allowable Pareto percentage is set to 70 %, and convergence stability percentage is set to 1 %. The measures defined in Equations (6) and (7) are used as two equally important minimization objective functions. The algorithm converged in 11 iterations with 1 % Pareto percentage and 0.59 % stability percentage, giving three candidate points shown in Table 6. The three candidate points give us fairly close parameter values (within 3.3 % range) so the choice

for further observation is somewhat arbitrary. We advance with the CP1 as it gives the lowest δ_{freq} and δ_{MAC}.

The results of the calibrated FE model are shown in Tables 7 and 8, together with the results of the initial FE model and experimental data for comparison. The results are also presented with FMAC plot in Figure 14, which should be compared to FMAC plot of the initial model in Figure 9. It is apparent that all modes have improved in regard to the initial model. Most significant improvement is seen in the shape of the 3rd mode and natural frequencies of the 4th and the 5th mode. It is also worth noting that the differences in natural frequencies are comparable to the discretization error, estimated in Section 3. From the MAC matrix in Figure 13, computed with the results of the calibrated model, one can see that the calibration process also improved the order of numerical modes. If we exclude 6th to 9th numerical mode of the new MAC matrix (which are modes with emphasized local deformations), it has a strong resemblance to experimental Auto-MAC matrix from Figure 8a, even in non-diagonal terms, which is a supporting indication that we have tackled the problem of spatial aliasing successfully.

5.6. Discussion on the results of FE model updating

The values of the parameters for the updated model need to be interpreted. The parameter e_1 is calibrated to 50.9 % of the initial value. This is a large discrepancy to account only for the uncertainty of the material property E_1. As expected, e_1 captures also the effect of the wall-floor joint explained in Section 5.2. With that in mind, the calibrated value for e_1 seems as a reasonable solution.

The parameters e_2 is within the expected interval. In particular, e_2 is 4.6 % higher than what is claimed by the CLT producer for E_1, and we can attribute the difference to the uncertainty of this material property.

This cannot be said, however, for e_3, which is 26.2 % lower that the initial value. The parameter e_3 captures also the in-plane flexibility of the floors due to connections, which is discussed in Section 5.3. Large in-plane flexibility of the floors for some modes can be partly attributed to the specific floor plan of Yoker building, with small rectangular area between the "web" and the "flange" of the T-like floor (see Figures 2 and 6). The difference in rotation of the "web" and the "flange", and the in-plane deformations of the floors, which are visible for modes 4 to 6 in Table 3, might suggest a small slip between the floor panels for the imposed vibration amplitudes during the test.

It is obvious that the parameter g_2 captures even more the large in-plane flexibility of the floors, because it settles at 47.6 % of the initial value. It is worth noting that g_2 significantly effects the 5th mode, but also the 4th and slightly the 6th mode, while it effects negligibly the first three modes, see Figure 12. In other words, the frequencies for the first three modes are almost not affected by the change of the value for g_2, while the frequencies for the last three modes are affected much more.

A large 61.7 % discrepancy between the increased calibrated and the initial value is also seen for g_1 (its initial value relates to G_{12} of the wall layers). It should be recalled that uncertainty in the material parameter G_{12} is large. In particular, the mean value that was claimed by the producer Stora Enso and the mean value proposed in EN-338 are considerably different, see Table 2. For comparison, the calibrated value for g_1 is only 7.8 % higher than the value given in EN-338, and 14.5 % higher than

650 MPa listed in [7] for CLT with narrow face bonding (this is the type of CLT produced by Stora Enso). The above suggests that the calibrated result for g_1 is not only a consequence of stochastic nature of G_{12}, but also that all sources of the wall-type stiffness might not be taken into account in the initial model. Recall that the stiffness of the non-load-bearing partition walls is neglected, as well as the stiffness of the cladding (and windows).

The change of the uncertain mass parameter q contributes to 2.59 % increase of the estimated initial mass of the building (1270 t). This is a reasonable value, which suggests that the additional mass did not compensate for a loss in the overall stiffness of the building during the FE model updating.

We can conclude that the calibrated values for the parameters from Table 6, except the one for e_2, include the effects of the modelling error. Thus, the calibrated values for e_1, e_3, g_1 and g_2 are not material properties. The modelling error is the most pronounced for e_1 (due to wall-floor joints) and for g_2 (due to large in-plane flexibility of the floors that may be attributed to the joints between the panels). Parameter g_1 may also include some modelling error, while large in-plane flexibility of the floors is captured also by e_3.

Table 6: Values of input parameters and objective functions of initial model and of three candidate points for solution of model updating.

Parameter	Initial model	CP1		CP2		CP3	
		Value	% of initial	Value	% of initial	Value	% of initial
e_1 [GPa]	12	6.11	50.9 %	6.23	51.9 %	6.24	52.0 %
e_2 [GPa]	12	12.55	104.6 %	12.45	103.8 %	12.57	104.8 %
e_3 [GPa]	12	8.85	73.8 %	8.98	74.8 %	8.98	74.8 %
g_1 [MPa]	460	744.1	161.7 %	748.0	162.6 %	747.8	162.6 %
g_2 [MPa]	460	219.0	47.6 %	216.1	47.0 %	212.0	46.1 %
q [kg m^{-2}]	25	36.63	+2.59 %[1]	36.88	+2.64 %[1]	36.37	+2.53 %[1]
δ_{freq} [$\times 10^{-3}$]	74.9	1.87		1.90		1.92	
δ_{MAC} [$\times 10^{-2}$]	58.1	4.53		4.83		4.87	

[1] Difference from initial model presented as a percentage of estimated initial mass of the building.

Table 7: Comparison of initial and updated model with experimental data.

Experiments	Initial model			Updated model		
Frequency	Frequency	Deviation	MAC_i	Frequency	Deviation	MAC_i
2.85	2.85	0.11 %	0.77	2.84	−0.41 %	0.83
2.93	2.81	−4.10 %	0.77	2.95	0.72 %	0.99
3.13	2.94	−6.07 %	0.38	3.08	−1.54 %	0.97
3.63	3.98	9.64 %	0.95	3.77	3.75 %	0.96
6.73	8.32	23.6 %	0.80	6.70	−0.46 %	0.95
8.74	8.19	−6.64 %	0.78	8.64	−1.16 %	0.90

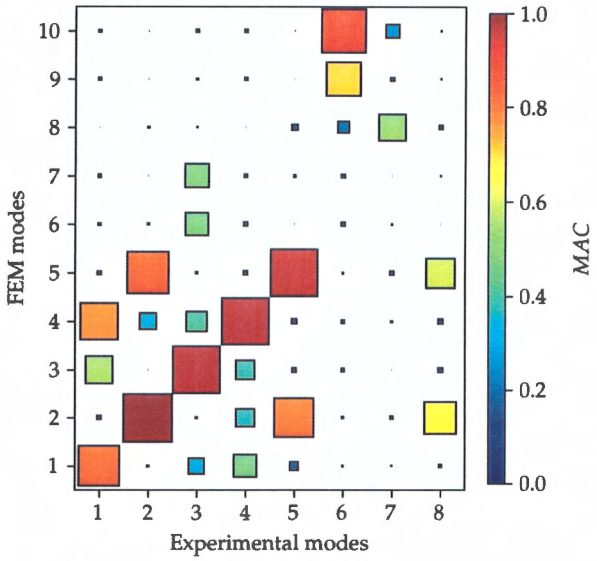

Figure 13: MAC matrix of calibrated model.

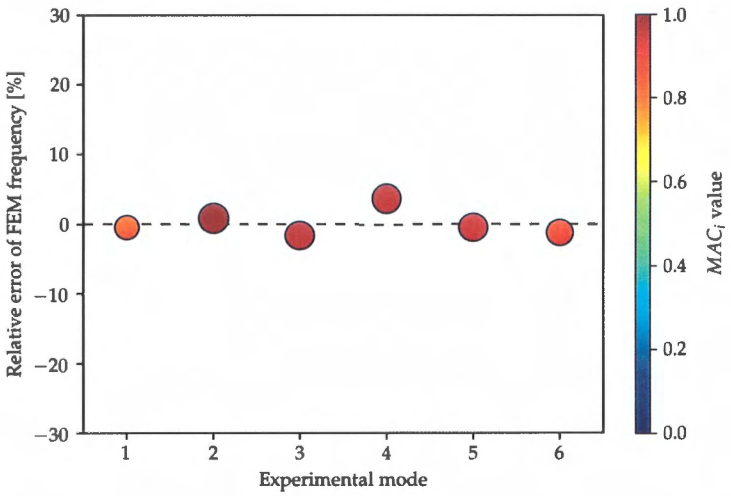

Figure 14: FMAC plot of the calibrated model.

Table 8: Graphical comparison of initial and updated model with experimental data.

Experiments	Initial model	Calibrated model
$f_1 = 2.85\,\text{Hz}$	$f_1 = 2.85\,\text{Hz}$, $MAC_1 = 0.77$	$f_1 = 2.84\,\text{Hz}$, $MAC_1 = 0.83$
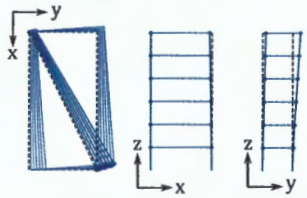	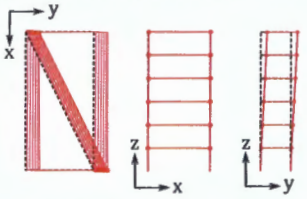	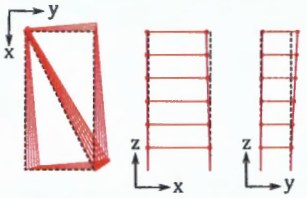
$f_2 = 2.93\,\text{Hz}$	$f_2 = 2.81\,\text{Hz}$, $MAC_2 = 0.77$	$f_2 = 2.95\,\text{Hz}$, $MAC_2 = 0.99$
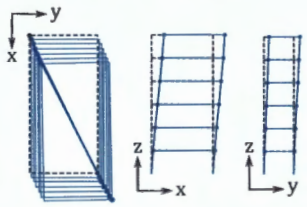	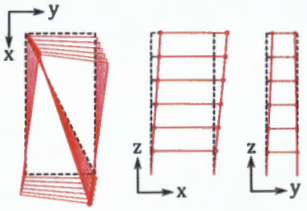	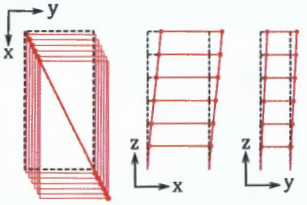
$f_3 = 3.13\,\text{Hz}$	$f_3 = 2.94\,\text{Hz}$, $MAC_3 = 0.38$	$f_3 = 3.08\,\text{Hz}$, $MAC_3 = 0.97$
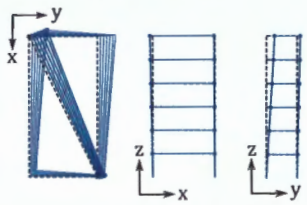	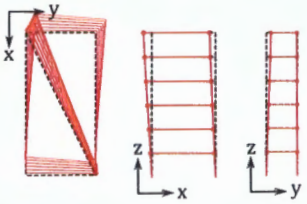	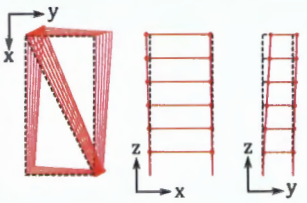
$f_4 = 3.63\,\text{Hz}$	$f_4 = 3.98\,\text{Hz}$, $MAC_4 = 0.95$	$f_4 = 3.77\,\text{Hz}$, $MAC_4 = 0.96$
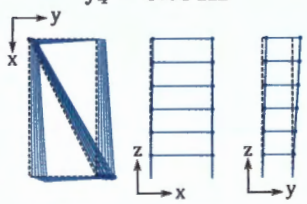	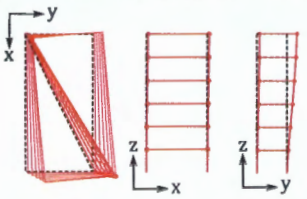	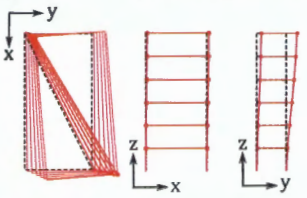
$f_5 = 6.73\,\text{Hz}$	$f_5 = 8.32\,\text{Hz}$, $MAC_5 = 0.80$	$f_5 = 6.70\,\text{Hz}$, $MAC_5 = 0.95$
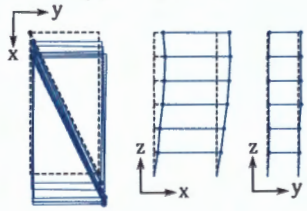	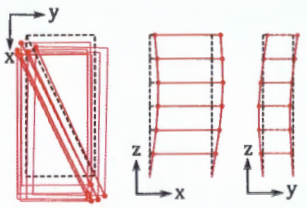	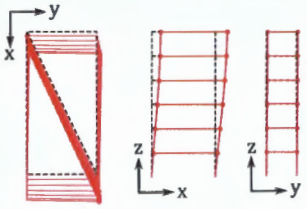
$f_6 = 8.74\,\text{Hz}$	$f_6 = 8.19\,\text{Hz}$, $MAC_6 = 0.78$	$f_6 = 8.64\,\text{Hz}$, $MAC_6 = 0.90$
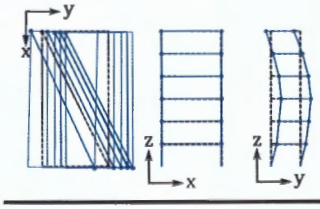	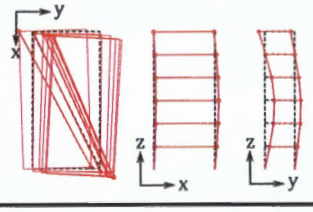	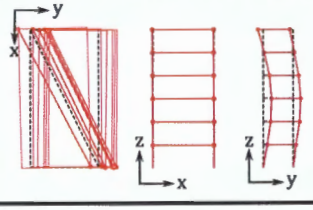

6. Including foundation in the model

In the above presented FE models, the foundation was considered as rigid and fixed. In this section, we will change the initial FE model by taking into account (in an approximate manner) the flexibility of the foundation and its interaction with soil. By performing updating of in such way improved initial model, we will check for the effect of the foundation on the dynamic response of the building.

The foundation of Yoker building can be described as follows. The reinforced concrete ground floor slab of thickness 175 mm sits on the top of a system of short reinforced concrete walls of height 850 mm and thickness 215 mm (in the middle area and 140 mm on the edges). The walls are on their bottom edge connected to the reinforced concrete horizontal frame with the square cross-section of 600 mm × 600 mm. Underneath the frame, there are 135 reinforced concrete piles with diameter of 250 mm and lengths of approximately 9 m.

6.1. Foundation modelling

We model the ground floor slab and the walls below it with shell finite elements, and the horizontal frame with beam finite elements. The data for the reinforced concrete are: density $\rho = 2300\,\mathrm{kg\,m^{-3}}$, modulus of elasticity $E = 32\,\mathrm{MPa}$ and Poisson's ratio (for the shell elements) $\nu = 0.18$. The effect of the pile and the pile-soil interaction were taken into account by three orthogonal springs located at the point where pile is attached to the horizontal frame. The stiffness of the horizontal and vertical spring is denoted as k_h and k_v, respectively. Moreover, the interaction between the foundation wall system (and frame) and soil is taken into account by the horizontal area spring with stiffness k_d. The foundation part of the FE model is illustrated in Figure 15.

Stiffness values for the above introduced springs are very uncertain, but some rough estimates can be made based on the geometrical and material properties of the piles and estimated elastic modulus of the soil by taking into account suggestions from [32]. The elastic modulus of the soil was estimated from twelve quick undrained triaxial compression tests on different locations under the building, giving us values between 0.9 MPa and 21.1 MPa with average of 6.1 MPa. Using those values to estimate the stiffness of the springs (see [32]) gives us from $1.9 \times 10^3\,\mathrm{N\,mm^{-1}}$ to $2.3 \times 10^4\,\mathrm{N\,mm^{-1}}$ for k_h and from $7.9 \times 10^3\,\mathrm{N\,mm^{-1}}$ to $1.4 \times 10^5\,\mathrm{N\,mm^{-1}}$ for k_v. Another estimate for the vertical stiffness of pile is obtained by treating the pile simply as the bar and get $k_v = \frac{E_p A_p}{L_p}$ from elastic moduli, cross-section area and pile length. For the previously given pile data, this gives us $k_v = 1.67 \times 10^5\,\mathrm{N\,mm^{-1}}$.

6.2. Updating of the model with foundation

The FE model updating is repeated for the initial model that takes into account the foundation. The stiffness of the springs, k_v, k_h and k_d, are added to the six parameters from Table 5 that were used for the updating of the model without foundation. To choose the range of the three newly introduced parameters and to get some more knowledge about these parameters, linear (one-at-a-time) sensitivity analysis has been carried out (by using the calibrated model from Section 5.5). For each parameter, a threshold value was found, above which the FE model behaves as if the corresponding degrees of freedom (either vertical or horizontal) are fixed, see Figure 16. We have chosen this threshold to be the

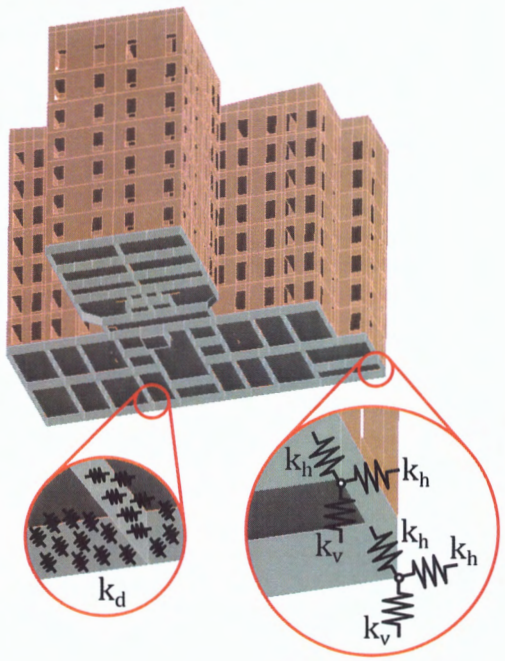

Figure 15: Modelling of the foundation.

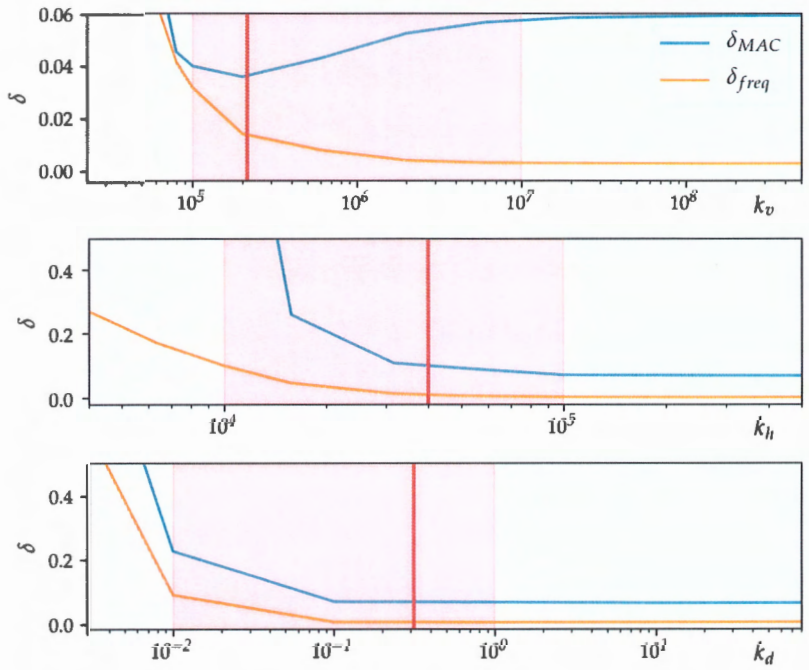

Figure 16: One-at-a-time sensitivity analysis for the spring stiffness parameters. Parameter range for model updating is shaded in red. The calibrated value is presented with red vertical line.

upper bound of the parameter range for the second model updating presented below. Sensitivity analysis also suggests that lowering the stiffness of the parameters k_h and k_d worsens the results obtained by the first updating from Section 5.5, while the value of parameter k_v below the threshold slightly improves the mode shapes obtained by that updating. Values $1 \times 10^4\,\mathrm{N\,mm^{-1}}$ for k_h, $1 \times 10^5\,\mathrm{N\,mm^{-1}}$ for k_v and $1 \times 10^{-2}\,\mathrm{N\,mm^{-3}}$ for k_d were selected for lower bounds of the parameter ranges, as they result in unreasonably low natural frequencies.

The ranges for the three new parameters are given in Table 9. The six parameters from the previous analysis, as defined in Table 5, are also included in the second model updating. The data for these parameters remains the same, except for the range of uncertain mass q, which is extended from -50 to $100\,\mathrm{kg\,m^{-2}}$ for the case that the optimization algorithm would compensate for the loss of stiffness in foundation. Negative value for the uncertain mass parameter would obviously mean reduction of the estimated initial mass of non-structural elements acting on the same areas as uncertain mass. Thus, a negative value for the uncertain mass would compensate also for the variance in timber density (from the value taken from the design documentation) and discrepancy of weight of non-structural elements from the documented values.

Table 9: Additional parameters due to modelling of foundation and their ranges for the second model updating.

Parameter	Range	Description
k_h	10^4–$10^5\,\mathrm{N\,mm^{-1}}$	Stiffness of horizontal springs on locations of piles.
k_v	10^5–$10^7\,\mathrm{N\,mm^{-1}}$	Stiffness of vertical springs on locations of piles.
k_d	10^{-2}–$1\,\mathrm{N\,mm^{-3}}$	Horizontal area spring stiffness on the foundation walls.

Table 10: Values of input parameters and objective functions of initial model and of three candidate points for solution of the second model updating.

Parameter	Initial model	CP1		CP2		CP3	
		Value	% of initial	Value	% of initial	Value	% of initial
e_1 [GPa]	12	7.17	59.8 %	8.52	71.0 %	7.16	59.7 %
e_2 [GPa]	12	11.38	94.8 %	10.87	90.6 %	10.34	86.2 %
e_3 [GPa]	12	8.42	70.2 %	6.76	56.3 %	7.77	64.8 %
g_1 [MPa]	460	726.1	157.8 %	741.5	161.2 %	704.8	153.2 %
g_2 [MPa]	460	213.0	46.3 %	210.7	45.8 %	213.0	46.3 %
q [$\mathrm{kg\,m^{-2}}$]	25	-2.95	−6.22 %[1]	-6.95	−7.11 %[1]	-2.61	−6.15 %[1]
k_v [$\mathrm{N\,mm^{-1}}$]		2.14e5		1.52e5		2.16e5	
k_h [$\mathrm{N\,mm^{-1}}$]		4.00e4		6.87e4		3.88e4	
k_d [$\mathrm{N\,mm^{-3}}$]		0.315		0.191		0.317	
δ_{freq} [$\times 10^{-3}$]	74.9	4.09		4.83		5.36	
δ_{MAC} [$\times 10^{-2}$]	58.1	4.72		4.65		4.83	

[1] Difference from initial model presented as a percentage of estimated initial mass of the building.

As in the calibration from Section 5.5, multi-objective genetic algorithm was selected for optimization in Ansys. Due to longer computation times, we set the number of samples for the initial and all other iterations to 75 with the limit on 12 iterations. Maximum allowable Pareto percentage is set to 70 %, and convergence stability percentage is set to 1 %. Objective functions from Equations (6) and (7) remain the same as for the first updating. The algorithm converged in 9 iterations with 1.33 % Pareto percentage and 0.65 % stability percentage, giving three candidate points shown in Table 6. Objective function δ_{MAC} for all three candidate points is fairly similar, whereas δ_{freq} slightly varies. We select CP1 as it gives the lowest δ_{freq}, see Table 10.

6.3. Discussion on the results of the second FE model updating

The resulting values of the old parameters are close to those from the first model updating (compare CP1 in Tables 10 and 6). There is a change for e_1, where previously calibrated result (50.9 %) changed to 59.8 % of the initial value, wich is still a reasonable solution according to the discussion in Section 5.6. Differences in other stiffness parameters are either not very significant (within 5 % from the first updating for parameters e_3, g_1 and g_2) or they are around the mean value of the material parameter (5.2 % less than the initial value for e_2). We can conclude that for the parameter values for e_1, e_2, e_3, g_1 and g_2 from Table 10, the observations stated in Section 5.6 still hold and that the values from the second updating are reasonable.

The uncertain mass parameter q settles at a value $-2.95\,\mathrm{kg\,m^{-2}}$, which in effect reduces the estimated initial mass of the building by 6.22 %. Comparing with the uncertain mass $q = 36.63\,\mathrm{kg\,m^{-2}}$, which is the result of the first updating from Section 5.5, the second updating suggests that the total mass of the building (without ground floor slab and foundation) is 91 % of the total mass resulting from the first updating. This is still within the reasonable bounds for the timber building, having in mind that even the mean value for the C24 spruce density varies for more that 10 % between the relevant documents, see Table 2.

The newly introduced parameters give some insights how the foundation might behave under small amplitude and low frequency range dynamic excitations. The two horizontal spring stiffness parameters (k_h and k_d) have settled on values near the upper bound, where the horizontal motion is almost completely restrained. Thus, the second FE model updating suggests that the horizontal motions of the foundation system are negligible. In contrast, vertical spring stiffness parameter k_v settles at a value that allows some movement according to the sensitivity analysis in Figure 16. The value of the vertical stiffness k_v is 28 % higher than estimated by axially loaded bar simplification, where $k_v = 1.67 \times 10^5\,\mathrm{N\,mm^{-1}}$.

The remaining results of the second updating, i.e. natural frequencies and MAC values, are presented in Figures 17 and 18. They are compared with the results of the first updating in Table 11. For comparison with the first updating check also MAC matrices from Figs. 13 and 17 and FMAC plots from Figs. 14 and 18. The results show that by adding foundations to the FE model, we have not improved matching the experiments. In the terms of the mode shapes, we have slightly improved matching the first, but worsened the sixth mode shape. We have also not improved matching of the natural frequencies either. However, the overall results of the second updating for frequencies and

MAC values are only slightly worse (with respect to the experimental results) from those obtained in the first updating.

We can thus conclude from the above results that for low frequency range (2 Hz–10 Hz) and for small amplitude dynamic response (0-0.005 m/s^2), modelling of foundation is not necessary for Yoker building.

Table 11: Comparison of results of two model updatings.

Experiments	1st updating			2nd updating		
Frequency	Frequency	Deviation	MAC_i	Frequency	Deviation	MAC_i
2.85	2.84	−0.41 %	0.83	2.79	−2.11 %	0.88
2.93	2.95	0.72 %	0.99	2.88	−1.71 %	0.99
3.13	3.08	−1.54 %	0.97	3.02	−3.51 %	0.96
3.63	3.77	3.75 %	0.96	3.79	4.41 %	0.96
6.73	6.70	−0.46 %	0.95	6.80	1.04 %	0.95
8.74	8.64	−1.16 %	0.90	8.70	−0.46 %	0.84
δ_{freq} [$\times 10^{-3}$]		1.87			4.09	
δ_{MAC} [$\times 10^{-2}$]		4.53			4.72	

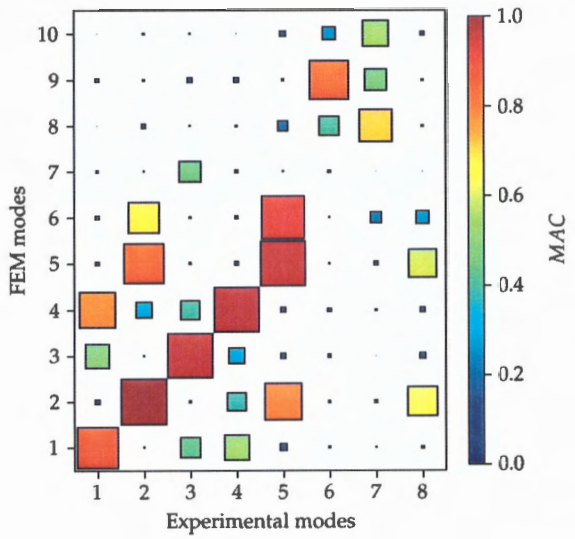

Figure 17: MAC matrix of the 2nd updated model.

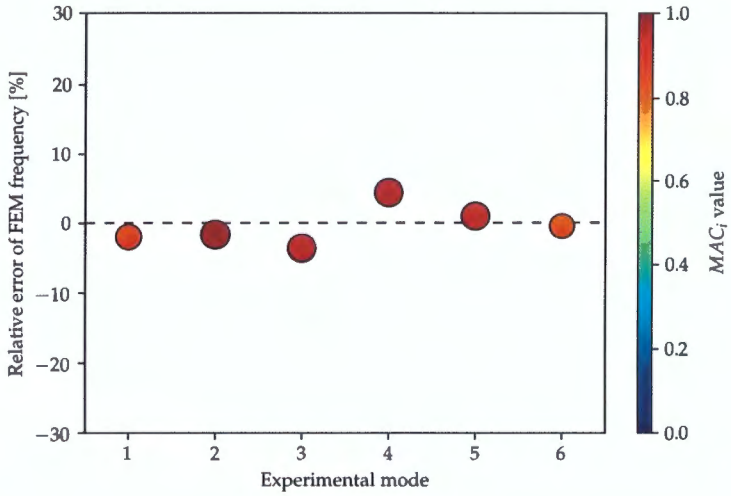

Figure 18: FMAC plot of the 2^{nd} updated model.

7. Conclusions

The best-engineering-judgement on FE model (initial FE model) of a seven-storey CLT building was built. The use of the preliminary FE results were compared to the results of the forced vibration test (FVT). The FVT was performed in order to identify the building dynamic properties under service dynamic loadings FIX: loading or loadings? with small amplitudes (i.e. wind actions FIX: what action? and action or actions? not clear! or you want to say wind load). FIX: I thought here you missed a sentence to describe why you need to do FE model updating. e.g.: However, the results of preliminary FE model was not shown consistent dynamic properties to the measurement. Furthermore, sensitivity analysis and deterministic FE model updating were carried out, which resulted in successful matching of first six modes. Spatial aliasing was present in the vibration tests, which overcame by using auto-MAC matrix FIX: I don't think spatial aliasing is a right use definition here, please rewrite it and this sentence doesn't make sense .

The initial FE model took into account the stiffness of the load-bearing elements of the building. FIX: The assumption that the floors act as rigid diaphragms was not adopted, rather the floors were modelled as flexible <– I couldn't link this sentence to the first sentence, please add more information. The connections and the soil-structure interaction were not taken into account. As for the non-load-bearing partition walls (which were not made of CLT panels), their stiffness was not considered as they were only approximately 6 % of the total walls (in mass percentage) per storey. On the other hand, the dead mass of all building elements (including the non-load-bearing ones) was considered carefully by using the design documentation in order to have the FE model with adequately realistic mass. The CLT structure of the building was discretised with a fine mesh of layered shell elements. The global discretisation error of the used mesh was below 2 %. The FIX: match <–do you mean "difference"? between the six experimental and numerical frequencies of the initial FE model

was within 24 %. However, the fundamental bending and torsion modes could be made a distinction (the first three modes and also the sixth mode) that exhibited better frequency matching (below 7 %) and more complex modes (modes 4 and 5) that did not match well. A clear difference between the fundamental and complex modes was that the latter also showed in-plane (shear) deformations of floor slabs.

The conclusion from the initial FE model study may be the following. The basic bending and torsion modes of a tall CLT building can be predicted within a reasonable error (below 10 %) with the FE model that do not take into account the connections (neither the stiffness reduction due to the wall-floor joint) if the following conditions are met: (i) A fine mesh of FEs is used (with the discretisation error in the range of 2 % in our case), (ii) The percentage of the non-load bearing partition walls, which stiffness was not included in the model, is small (in the range of 6 % in our case), (iii) The dead mass of the building is carefully estimated from the design documents, and (iv) Mean values for the material parameters FIX: e.g. ? are used (as provided by CLT producer in our case). Although FIX: what is the subject? not checked numerically, the floors were modelled as flexible FIX: flexible of what? a bit not clear, please clarify in our study. From the sensitivity analysis, the assumption of floors behaves as rigid diaphragms, which is not unreasonable for the lower basic modes. However, all the external walls and some of the internal walls of the building are composed storey-wise of large CLT panels (which length equals the length of the edge of the building) with pre-cut openings, while other arrangements for the walls with smaller CLT panels that would likely increase the error FIX: of what? modelling error? and what is the solution to fix the error? .

By choosing the updating parameters, which take into account, in a smeared sense, the effect of wall-floor joints and the effect of floor connections, the deterministic FE model updating was performed. First six frequencies of the updated FE model match with the experimental measurement within 1.5 % difference, except for one frequency which matches to 3.75 %. This result suggests that the floor connections and the wall-floor joints do have a considerable influence on the overall stiffness of the CLT building under service loadings, though more for the complex modes than for the basic bending and torsion modes.

To check the effect of the foundation and the soil-structure interaction, the updating procedure was repeated on a FE model with foundation, the latter being modelled with a set of springs element. The previously computed updated frequencies change only slightly, demonstrating that for small amplitude and low frequency dynamic response of the observed building the foundation and the soil-structure interaction modelling was not mandatory.

The main conclusion from the presented study may be the following. The connections do have a considerable impact on the overall behaviour of tall CLT buildings under dynamic service loadings with small amplitudes (e.g. wind). In this respect, two influential sources of stiffness reduction have been identified by the FE model updating: the wall-floor joints and the floor connections. The former influence the overall stiffness of the CLT walls, while the latter have a large impact on the in-plane stiffness of the CLT floors. Our results show that the application of the rigid-diaphragm assumption for the CLT floors is not justified, at least for any mode that is not the basic one. Consequently, a FE model with a good prediction capacity for dynamic behaviour of tall CLT building at small amplitudes,

which incorporates the basic dynamic properties of such a building in a realistic manner, should take into account the influence of the two above mentioned connection details. Indeed, the requirements (i) to (iv) listed above apply for such FE model. Also, modelling the effects of the connection details in this work was not given much variation of the FE results.

Acknowledgments

The research was done in the framework of Dyna TTB project. The financial support of ERA-NET Cofund Forest Value and the corresponding funding bodies is gratefully acknowledge. We also thank F. Perez, the designer of Yoker building, from Smith and Wallwork Ltd at Cambridge, UK, for design documentation and many helpful discussions, and B. Pulko for helpful suggestions regarding foundation modelling.

8. Bibliography

[1] Ansys® Academic Research Mechanical, Release 2020 R1.

[2] European technical assesment ETA-14/0349 of 03.06.2019. Technical report, Austrian Institute of Construction Engineering, 2019.

[3] R. Allemang. The modal assurance criterion – twenty years of use and abuse. *Sound and Vibration*, 37(8):14–21, 2003.

[4] A. Aloisio, D. Pasca, R. Tomasi, and M. Fragiacomo. Dynamic identification and model updating of an eight-storey CLT building. *Engineering Structures*, 213(March):110593, 2020.

[5] E. Borgonovo and E. Plischke. Sensitivity analysis: A review of recent advances. *European Journal of Operational Research*, 248(3):869–887, 2016.

[6] R. Brandner, P. Dietsch, J. Dröscher, M. Schulte-Wrede, H. Kreuzinger, and M. Sieder. Cross laminated timber (CLT) diaphragms under shear: Test configuration, properties and design. *Construction and Building Materials*, 147:312–327, 2017.

[7] R. Brandner, G. Flatscher, A. Ringhofer, G. Schickhofer, and A. Thiel. Cross laminated timber (CLT): overview and development. *European Journal of Wood and Wood Products*, pages 1–21, 2016.

[8] B. Brank and E. Carrera. Multilayered shell finite element with interlaminar continuous shear stresses: a refinement of the reissner–mindlin formulation. *International Journal for Numerical Methods in Engineering*, 48:843–874, 2000.

[9] B. Brank, F. B. Damjanić, and D. Perić. On implementation of a nonlinear four node shell finite element for thin multilayered elastic shells. *Computational Mechanics*, 16:341–359, 1995.

[10] G. D'Arenzo, D. Casagrande, T. Reynolds, and M. Fossetti. In–plane elastic flexibility of cross laminated timber floor diaphragms. *Construction and Building Materials*, 209:709–724, 2019.